Influence of local mechanical loading paths on the oxidation assisted crack initiation of alloy 718

Benoît Ter-Ovanessian[a,b,*], Dominique Poquillon[b], Jean-Marc Cloué[a], Eric Andrieu[b]

[a] AREVA, AREVA NP 10, rue J. Récamier, 69456 Lyon Cedex 06, France
[b] Université de Toulouse, CIRIMAT, INP/UPS/CNRS, INP-ENSIACET, 4, allée Emile Monso - BP 44362 - 31030 TOULOUSE Cedex 4, France

A B S T R A C T

At high temperatures, alloy 718, like many other nickel-based superalloys, is sensitive to an oxidation-assisted intergranular crack (OAIC) growth mechanism. Former studies have pointed out that even if intergranular oxidation still occurred, intergranular crack initiation was inhibited due to specific mechanical loadings which were identified as Portevin-Le Châtelier (PLC) plastic instabilities. In the present work, key parameters triggering crack initiation or PLC instabilities in the [550–700 °C] temperature range were determined for the studied grade by means of tensile tests on smooth specimens. Then, in order to assess the applicability of such a finding at a scale compatible with the material microstructure, a dedicated tensile V-shaped specimen was designed to generate different surface and sub-surface strain and strain rate histories. Thanks to a dual approach based on the observation of crack initiation location on this specific experimental specimen together with associated FE calculations, the critical mechanical loading paths inducing OAIC initiation have been specified. Thus, assuming that the metallurgical state is homogenous at the structure scale, a mapping of intergranular crack initiation is then obtainable.

Keywords:
Ni-based superalloys
Environment-assisted cracking
Portevin-Le Châtelier effect
Finite element simulation

1. Introduction

Alloy 718 is known to be sensitive to an oxidation assisted intergranular crack (OAIC) growth mechanism at temperatures close to those encountered industrially for turbo machine disks (650 °C-air) [1–9]. Recent work [6–9], investigating the detrimental effect of oxidation on the lifespan and the mechanical behaviour of alloy 718, has demonstrated that during tensile tests carried out under synthetic air at a 400–600 °C temperature range and at a $5 \times 10^{-7}\,s^{-1}$ to $10^{-1}\,s^{-1}$ strain rate range, the disappearance of the intergranular brittle area on the fracture surface systematically corresponded to the occurrence of Portevin-Le Châtelier (PLC) phenomenon. Moreover, the same tests carried out under inert atmosphere systematically exhibited a fully transgranular ductile fracture mode, whatever the plastic flow regime was. Although the occurrence of plastic instabilities (jerky flow, or Portevin-Le Châtelier phenomenon), and more generally dynamic strain ageing (DSA) during plastic flow of alloy 718 for such range of temperature is commonly observed [10–13], different hypotheses about their impact on oxidation assisted intergranular crack growth were proposed [6–9]. Among them, Fournier et al. [6], suggested that the correlation between the disappearance of the intergranular fracture mode with the occurrence of PLC instabilities was linked to the strong localization of the strain in the PLC bands giving rise to the ductile fracture mode. Garat et al. [7], established an experimental map including deformation modes (DSA–PLC) and fracture modes for a large range of strain rates and temperatures. From these results, the authors suggested that the propagation of a type C PLC band, which is initiated in areas of high strain/stress localization like grain boundaries or, at another scale, in the plastic zone at the tip of a propagating defect, could modify the local stress distribution. Thus, if the plastic zone in front of a defect is extended enough to include several grains, it becomes possible that the rate of the stress redistribution due to the instability occurrence induces either a change in the crack path or a crack arrest, hence preventing intergranular crack propagation.

Furthermore, the microstructure of alloy 718 is known to generate a high propensity to concentrate the shearing along a few slip planes per grain leading to noticeable deformation heterogeneity. When dealing with intergranular crack initiation at the surface of such a material, the localization of crack initiation sites remains an open question. As all of the surface/sub-surface grain boundaries exhibited intergranular oxidation, the answer might be found in the release of grain to grain strain incompatibilities at the free surface of the polycrystal where only some grain boundaries keep high stress levels susceptible to initiate an intergranular crack or

* Corresponding author at: Université de Toulouse, CIRIMAT, INP/UPS/CNRS, INP-ENSIACET, 4, allée Emile Monso - BP 44362 - 31030 TOULOUSE Cedex 4, France.
Tel.: +33 534323449; fax: +33 534323498.
E-mail address: benoit.terovanessian@ensiacet.fr (B. Ter-Ovanessian).

Table 1
Chemical composition of as-received alloy 718 [wt.%].

Al	C	Co	Cr	Cu	Fe	Mn	Mo	Ni	Nb+Ta	Si	Ti
0.48	0.034	0.022	18.3	0.009	Bal.	0.046	3.04	53.69	5.17	0.031	1.05

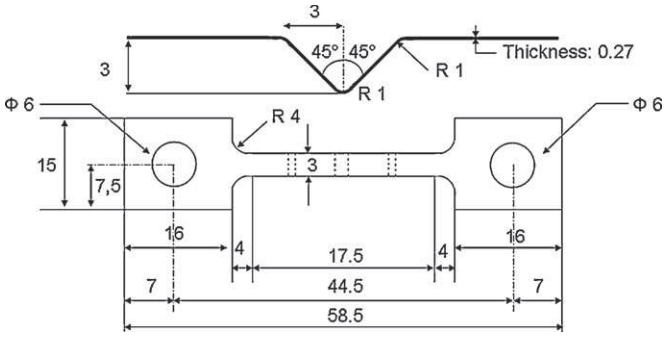

Fig. 1. Geometry of tensile specimens after cold stamping (dimensions in mm).

to be released by PLC instabilities. This type of approach assumes that the mechanical behaviour at the surface of the material is not very different from the bulk. In order to assess the validity of the approach, a dedicated tensile V-shaped specimen was designed to generate surface and sub-surface strain and strain rate gradients at a scale compatible with the material microstructure. Moreover, the improvement of the mechanical behaviour characterization of this V-shaped tensile specimen [8,14] highlighted the main advantages of this specific geometry in studying strain rate dependence of crack initiation. Indeed, this geometry enables to control the amount of material at the apex of the V submitted to the imposed strain rate [14]. As a result, the required loading conditions for crack initiation or for PLC bands generation are expected to be only fulfilled locally. Previously, Deleume et al. [14] already proved that, on a global scale, tensile tests' mechanical response and finite elements modelling were in good agreement for a similar geometry. However, from this preliminary study, it appeared necessary to obtain a complete description and evaluation of strain and strain rate gradients' distribution all along the tensile test in order to be better able to explain the localization of intergranular cracks observed at the end of the mechanical tests. The purpose of the present study is to provide this key information at 600 °C in order to accurately analyze the role of local loading paths (i.e.: critical strain, critical strain rate, plastic flow mode, etc.) on intergranular crack initiation behaviour of alloy 718.

2. Material and experimental procedures

The materials used in this study were obtained through a double melting process: vacuum induction melting plus electrode slag remelting. The nominal composition of the evaluated heat is given in Table 1.

The cast ingot was hot and cold rolled down to strips of 0.3 mm of thickness, followed by a solution annealing heat treatment at 1050 °C for one hour ended by air quenching. Thin tensile specimens were machined from the annealed strips. Then, while still at an annealed metallurgical state, V-shaped hump specimens were formed from tensile specimens, by cold stamping with a specific stainless steel dye (Fig. 1).

V-shaped specimens and conventional tensile specimens were then heat treated in an argon atmosphere following the conventional aeronautical route: hold at 720 °C – 8 h, cooling 50 °C/h down to 620 °C, hold at 620 °C – 8 h and final air cooling to room temperature. Such heat treatment aims at precipitating and stabilizing the hardening phases γ′ (Ni_3Al, average size 50 nm) and γ″ (Ni_3Nb, average size 15 nm × 50 nm).

All the mechanical tensile tests were performed on a hard electro-mechanical tensile machine with controlled displacement rate, outfitted with an environmental chamber, a radiation furnace and a laser extensometer. Two different types of tensile tests were carried out on thin flat conventional specimens under synthetic air or argon in the 550–700 °C temperature range for different imposed strain rates in the $10^{-5}\,s^{-1}$, $10^{-1}\,s^{-1}$ range. The first ones were carried out until failure whereas the second ones consisted in interrupted tests at a given plastic strain. After being tested, gage length and/or fracture surfaces were examined with a LEO 435VP scanning electron microscope (SEM). The purpose of the conventional tensile tests on thin flat specimens was to establish the mechanical behaviour of that specific grade at these temperatures and to determine the threshold value of disappearance/appearance of the PLC phenomenon. The purpose of the tensile tests interrupted at a given plastic strain was to evaluate the critical cumulated plastic strain necessary to observe crack initiation. For such interrupted tests, tensile specimens were heated then loaded until the wanted plastic strain was reached, then unloaded and finally cooled down. Then, SEM observations along the gage length allowed to detect crack initiation.

On the other hand, tensile tests have been carried out in similar testing conditions on V-shaped specimens. Some tests were carried out up to failure but other tests were interrupted for a given load corresponding to a given maximal plastic strain at the tip of the V. The purpose was to determine the localized mechanical behaviour of this specific geometry, without increasing stress triaxiality.

For both tensile specimens, the microstructure was characterized by equiaxed fully recrystallized small grains (ASTM grain size number = 8–9) with random grain boundaries and by the presence of some Nb/Ti carbide rows. Fig. 2 shows that the microstructure is homogeneous all across the V specimen thickness even in the most deformed parts.

Because of the cold stamping of the specimen, work hardening in the V-shaped is estimated by geometrical considerations to an average value of 13%. In order to evaluate the role of this work hardening on the subsequent behaviour of the V-shaped specimen for OAIC tests, tensile tests were carried out on tensile specimen which were pre-strained either at 12% or 20% at room temperature in the solution annealed state before being aged hardened. The mechanical response obtained, showed that the mechanical behaviour, at 600 °C, was not significantly modified by the previous work hardening. Therefore, only one flow rule may be used to characterize the whole behaviour of the V shaped specimen.

Finite element calculations were performed with Cast3 m finite element code [http://www-cast3m.cea.fr], in order to determine the local stress and strain tensor fields scale and distribution in the V-shaped specimen throughout the tensile tests. Because of the geometry (symmetry and width) of the specimen, the simulation was carried out using plane strain hypothesis and a 2D mesh (8 node-quadratic elements, corresponding to 9 μm × 9 μm) of half of the specimen. For calculations, the flow rule was described by an isotropic elastoplastic mechanical behaviour. Indeed, in Cast3m code, this mechanical behaviour with non-linear hardening enables to fit the true stress–strain curve.

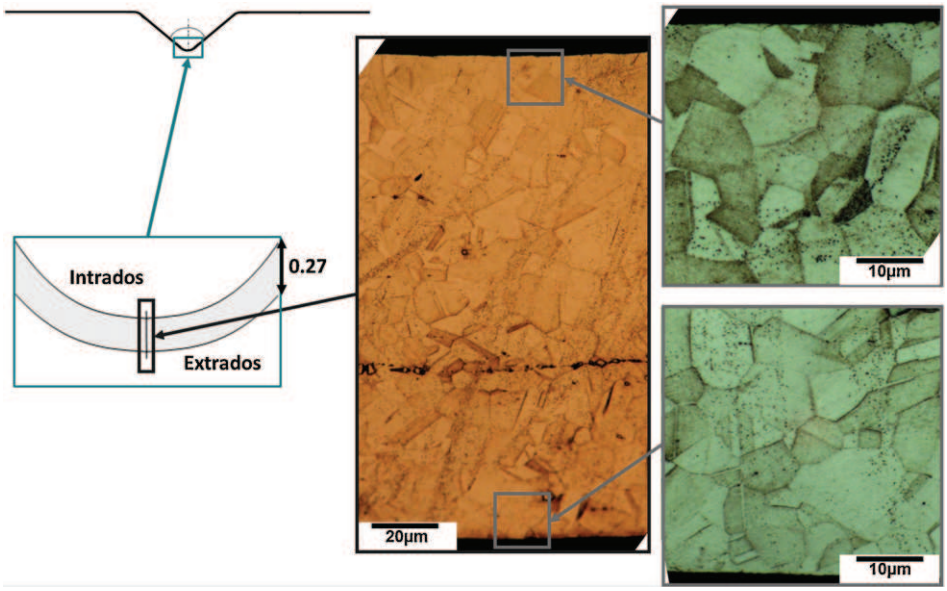

Fig. 2. Details of the microstructure at the apex of a V shaped tensile specimen after the forming process and the ageing heat treatment.

As a first result from thin tensile tests, in the investigated range of strain rates, the mechanical behaviour at 600 °C in the DSA regime did not significantly depend on the strain rate (Fig. 3); therefore, only a time-independent constitutive equation was required for finite element calculations to model the material behaviour in the samples.

A simulation was carried out opening the V sample until the applied load reached 60 N. From this step by step simulation up to 60 N, different local stain rates are deduced for the different displacement rates as detailed in Section 3.

3. Results

3.1. Tensile tests on thin tensile specimens

Tensile tests were carried out under air environment at 600 °C on conventional thin tensile specimen in order to determine the mechanical behaviour of this grade, for instance strain rate sensitivity of the flow stress. The results obtained, which are detailed in Fig. 3, indicate that the flow stress was not really modified by the strain rate while the ductility was. The fact that the flow stress is not (or few) sensitive to strain rate is not surprising in the DSA regime while the behaviour of the ductility seems to be specific to the studied case. Indeed, contrary to type A or B PLC phenomenon [15–19], the occurrence of type C PLC phenomenon is associated with an increase of the ductility [18,19]. Besides, such mechanical properties were obtained from tensile tests carried out under air for a narrow domain of strain rates. For higher strain rates, a decrease of the ductility could be observed.

Moreover, the scanning of the strain rate evidenced the threshold value of disappearance/appearance of the PLC phenomenon, which, in the present case, is in between $2.5 \times 10^{-4}\,s^{-1}$ and $3.5 \times 10^{-4}\,s^{-1}$. In addition, for the grade studied, Fig. 4 shows the obtained map in terms of plastic flow and rupture modes over a wider range of temperature. As previous work has already demonstrated [6–9], these threshold values corresponded to a transition in the fracture mode under air environment.

Furthermore, while PLC occurred, whatever the strain rate domain was, the serrations produced load drops below the general level of the stress–strain curve and the amplitude of the serrations was rather constant [7,9–13]. Both features characterized the type C of PLC phenomenon, according to Rodriguez's definition [19]. This

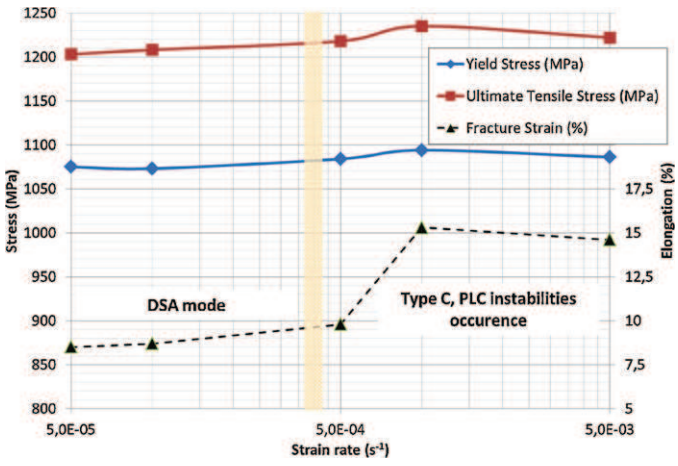

Fig. 3. Mechanical properties and deformation modes of studied materials at 600 °C from conventional tensile tests carried out for different strain rates under synthetic air.

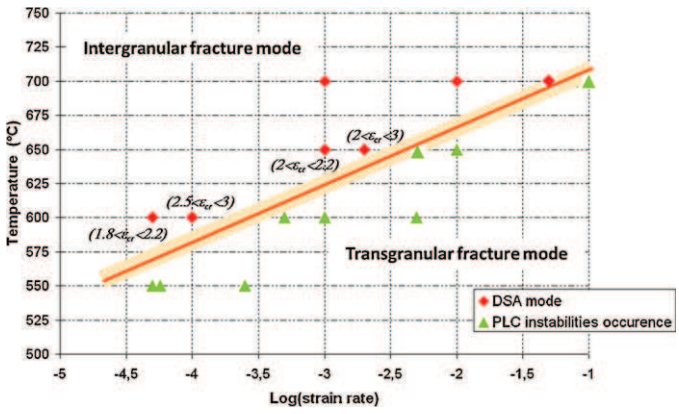

Fig. 4. Map of the rupture and plastic flow modes of the studied grade in the [550–700 °C] temperature range – in italics: the cumulated necessary deformation to initiate intergranular cracks.

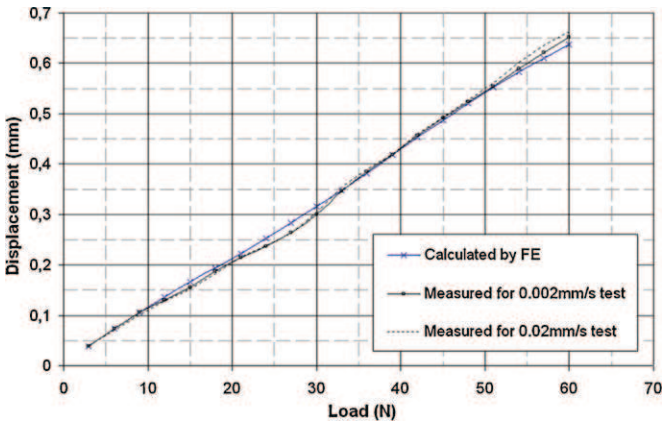

Fig. 5. Comparison of the predicted and the real global mechanical response of the specimen tested at 600 °C.

type is commonly associated with an audible emission and with the random nucleation of deformation bands all along the specimen gage [9,12,13,19]. The critical plastic strain for the onset of PLC instabilities was estimated to be between 0.20% and 0.60% for the entire PLC domain. Finally, in the DSA regime, thanks to the interrupted tensile tests at various levels of plastic strain and SEM examinations of the gage length, a plastic strain threshold value for the occurrence of crack initiation was determined. For the tested strain rates below the transition strain rate, at least 1.5% and at most 3% of cumulated plastic strain seemed necessary for crack initiation (in italics in Fig. 4).

3.2. Tensile tests on V-shaped specimens: experiments and global FE modelling

Up to failure tensile tests on V-shaped specimens were preliminarily performed in order to acquire the entire mechanical response of the specimen for different displacement rates of 0.2 mm/s, 0.02 mm/s and 0.002 mm/s at 600 °C. Indeed, as during the tensile test the strain rates changed from place to place due to the specimen geometry; it is more accurate to characterize the tests by using the imposed displacement rate. Tensile tests carried out at 0.2 mm/s and 0.02 mm/s led to a total opening up of the V followed by a transgranular ductile fracture. Conversely, tensile tests carried out at 0.002 mm/s were characterized by a premature failure occurring before the entire opening of the V associated with a mixed mode of fracture with intergranular brittle and transgranular ductile areas.

Complementary interrupted tensile tests were performed till the applied load reached 60 N with two imposed displacement rates (0.02 mm/s and 0.002 mm/s) in order to assess the ability of the finite element calculations with the chosen constitutive equations to reproduce the real mechanical behaviour of the specimen. FE simulation and real mechanical responses for both tests are presented in Fig. 5. It is worth noting that the curves illustrating the applied load as a function of displacement are very similar. These results are even more convincing as they make sense in another use of the model to describe the local aspects of the mechanical fields, step by step, especially strain and strain rate distribution as the tensile test proceeds.

Meanwhile, SEM examinations of the gage length for both displacement rates revealed that for interrupted tests carried out at 0.002 mm/s, cracks initiated at ~180 μm, ~220 μm and 260 μm from the apex of the V, while for interrupted tests carried out at 0.02 mm/s, no crack was detected. Fig. 6a and b illustrates some of the SEM observations after such an interrupted test.

3.3. Finite element modelling of local mechanical states

During the loading, the V tip is progressively opened. Thus, the inner part of the V is submitted to tension and is gradually strained. Previous work [14] has already focused on the strain gradient and its evolution during tensile tests in the apex of such a specimen. During the opening, as long as the angle changes between the arms

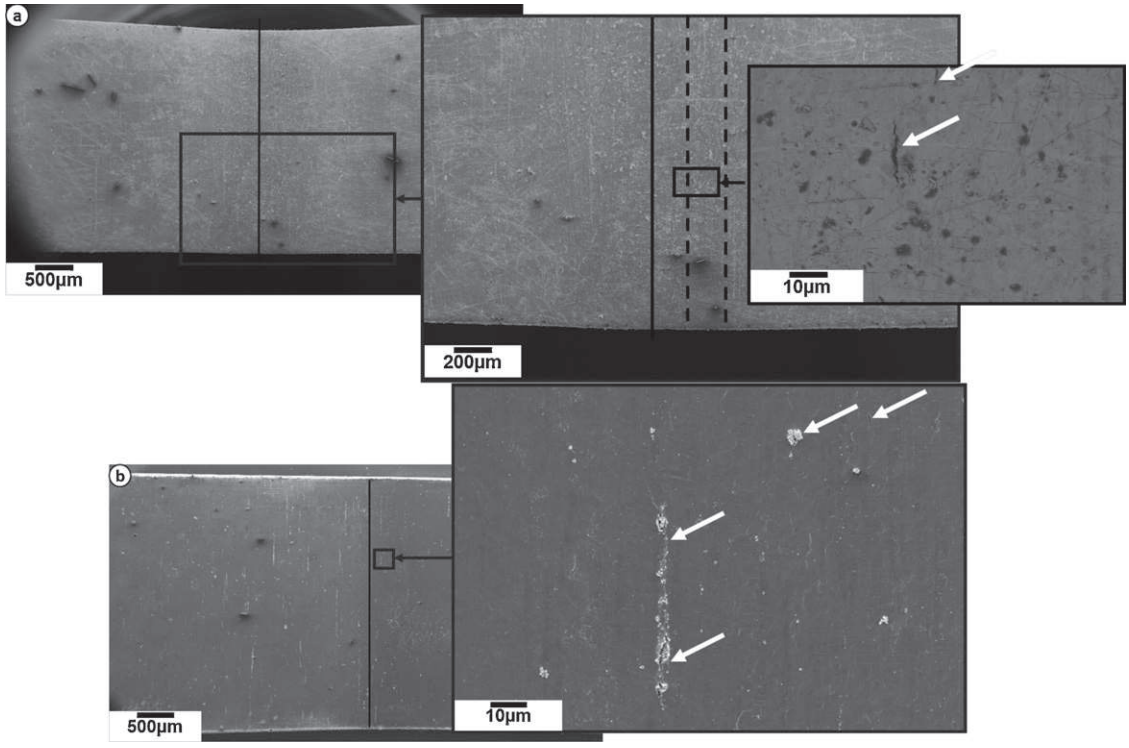

Fig. 6. (a) and (b) SEM observations and localizations of cracks initiated during two different interrupted tensile tests carried out at 0.002 mm/s on a V-shaped specimen.

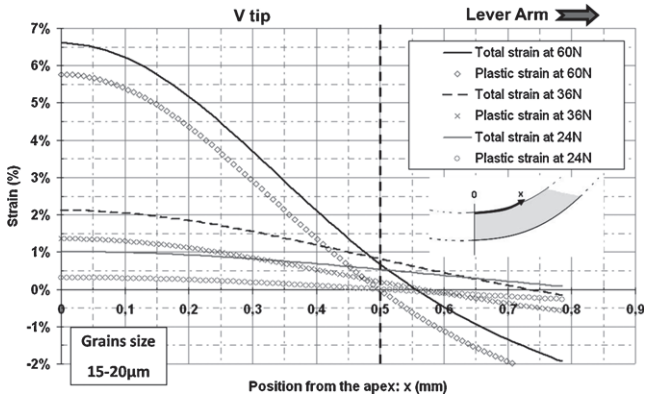

Fig. 7. Total and plastic strain in direction *x* at the intrados of the V as a function of the applied load. The distance *x* is given from the sample's plane of symmetry.

of the V remain small, an elastic approach can be used to access the strain evolution in the tip of the V [8,14]. However, when plastic straining occurs, it tends to be localized at the tip of the V and its contribution to total deformation becomes rapidly larger than the elastic one. For the studied specimen geometry, plastic strain contribution to the total deformation becomes higher than the elastic strain, once the applied load reaches $F = 36$ N (see Fig. 7). Increasing the load tends to localize the plastic strain more and more in the V, as shown by the shape of the curves in Fig. 7.

By considering an elastic approach and for a given displacement rate, the strain rate at the tip of the V is initially lower than the one obtained with a conventional tensile flat sample. This behaviour can be modelled by simple geometrical considerations [8,14]. However when considering plastic strain contribution, the previous elastic approach is no longer able to describe the local strain rate evolution as the tensile test proceeds. To go further in the analysis, simulated strain rate evolutions as a function of both location and displacement rate are presented in Figs. 8 and 9. The curves show that the strain rate increases progressively from the initial value to a plateau whose value depends on the position of the area of interest. Then, when opening the V, the stress distribution in the intrados surface changes so that finally the tip of the V reaches a strain rate which tends to reduce the crack initiation probability in this area.

Changing the loading rate changes the local strain rate but due to the insignificant strain rate sensitivity of the material in these mechanical testing conditions, the shape of the range of curves remains almost unchanged whatever the displacement rate is. For

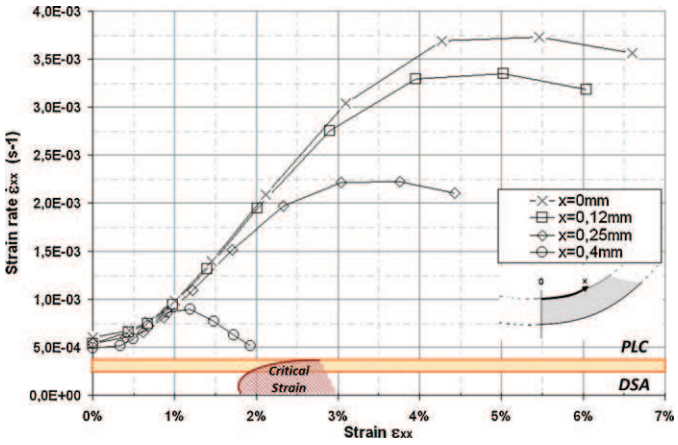

Fig. 8. Total strain–strain rate path followed by several areas of interest located at the tip of the V for a given displacement rate (0.02 mm/s). PLC/DSA boundary is superimposed with cumulated necessary strain to initiate intergranular cracks.

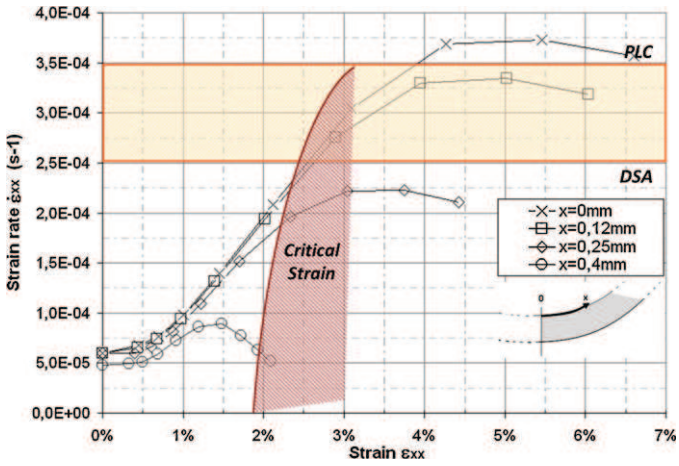

Fig. 9. Total strain–strain rate path followed by several areas of interest located at the tip of the V for a given displacement rate (0.002 mm/s). PLC/DSA boundary is superimposed with cumulated necessary strain to initiate intergranular cracks.

each case, different maps showing strain–strain rate paths followed by the material located in the apex of the V can easily be calculated. On these maps, the strain rate interval demarcating the disappearance/appearance transition of the PLC phenomenon together with the critical plastic strain interval were superimposed (in Figs. 8 and 9) in order to point out the boundary of the area inside which the damaging conditions at this temperature are fulfilled. An interrupted tensile test has been carried out at 0.02 mm/s up to an applied load of 60 N. These mechanical testing conditions reproduce the simulation conditions presented in Fig. 8. As previously mentioned, finite element calculations concluded that the damaging conditions were never fulfilled on the entire V since strain rates quickly reached the PLC instabilities domain before cumulating the critical plastic strain to initiate intergranular cracks. The fact that no crack was detected on the gage length of the tested specimen corroborates the finite element calculations. Finally, it also explains why the tests carried out up to rupture at 0.02 mm/s gave rise to a fully ductile fracture. Conversely, for an interrupted tensile test carried out at 0.002 mm/s, associated with Fig. 9, the finite element calculations predict that the crack initiation may occur over a wide area centred at 250 µm from the apex of the V. Observations of cracks initiated at ~180 µm, ~220 µm and 260 µm from the V apex on the corresponding interrupted tensile test specimen (see Fig. 6), seem to prove that experimental results and simulations are in good agreement and consequently that the specimen geometry is useful in investigating crack initiation conditions in alloy 718.

4. Discussion

Elastoplastic isotropic model used for FE calculations accurately leads to a local mapping of plastic strain and strain rate of the V thickness or of its extreme surface. Indeed, the area of interest in this study is a boundary layer at the tip of the V whose thickness is of the range of the microstructure size, on which damaging phenomena are beforehand modelled at a macroscopic scale. The striking fact that the probability domain of crack initiation evidenced by FE calculations and macroscopic experimental data exactly matches the crack localization from SEM observations on the gage length of the interrupted tensile tests implies that random phenomena generally observable macroscopically, like DSA/PLC phenomena or rule of damage accumulation, may be localized, in the present case, at the surface layer of the V structure. Indeed, these experiments confirm not only the relevancy of the use of such geometry for OAIC concerns, but also the possibility of a transposition of loading conditions inducing OAIC on the scale of a conventional tensile specimen

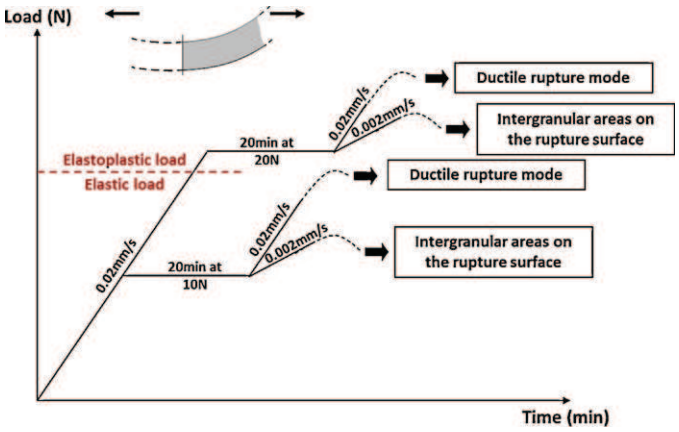

Fig. 10. Schematic loading paths and results of tensile tests carried out on V-shaped specimens at 600 °C under synthetic air.

to the scale of the inner surface of the tip of the V-shaped one. Thus, thanks to this transposition, the mechanical key parameters responsible for OAIC may be demonstrated and characterized.

The effect of the environment, in terms of intergranular oxidation and weakening reactions, is already proved to be a necessary, but not a sufficient component, of the damaging process [1–9]. However, if all of the grain boundaries are oxidized, the role of local stresses, cumulated strain, and strain rate still raises questions about their actions and interactions in the damaging process. The present results tend to minimize the direct role of the stresses on OAIC concerns for alloy 718 and conversely, emphasize the role of strain rate and plasticity. Firstly, the rupture mode map (Fig. 4) correlated with Fig. 2, showed that for similar flow stresses, the rupture mode changes principally as a function of the deformation mode, i.e.: the strain rate relating to pure DSA or PLC instabilities. Secondly, to activate OAIC mechanisms, a critical plastic strain accumulation seems to be required. Therefore, if this plastic strain is not cumulated thanks to a slow strain rate-DSA flow mode-crack initiation does not occur.

In order to understand and try to dissociate the effects of time and plasticity from the strain rate role on the OAIC process, complementary tests were carried out. A schematic representation of these new experiments is presented in Fig. 10. V-shaped tensile specimens were loaded at 10 N (elastic load) or 20 N, which is closed to the elastoplastic threshold of the V structure, with a displacement rate of 0.02 mm/s and maintained respectively at this load for 20 min. Then, after each load dwell, specimens were tested up to rupture at displacement rates of 0.02 mm/s or 0.002 mm/s. Fracture surfaces were observed by SEM.

The fact that for each tensile test performed at 0.02 mm/s after the load dwell, the fracture surface is totally transgranular ductile while for tensile tests performed at 0.002 mm/s after the load dwell, the fracture surface exhibits intergranular areas, demonstrates that the role of the strain rate is not entirely a temporal or diffusional role and that the plasticity component must be taken into account. Therefore, from a mechanistic point of view, the intergranular weakening of the material is not due to the simple diffusion of reactive species from the core of the grain to the grain boundaries or from the aggressive environment to the grain boundaries, but seems to be related to the high level of grain to grain strain incompatibilities and/or to interactions between plasticity and mobile species. Previous work [9] demonstrated that for tensile tests carried out, in similar testing conditions than those presented in this paper, on a low interstitial content alloy with similar mechanical properties, the transition DSA regime to PLC instabilities was no longer related to a modification of the fracture mode which remained transgranular. These results strongly suggest that interstitials species play a first order role in the OAIC process.

Such interactions between dislocations and solute species are known to occur during DSA and PLC regimes [10,15–24] in interstitial or substitutional alloys. However, in the case of age-hardenable alloys, another parameter must be taken into account to realize DSA/PLC regimes: the hardening precipitates. Indeed, precipitates have a significant effect on the dislocation mobility and on the characteristics of the pinning/pinning off effect (characteristic distance, characteristic time, etc.) [23,25]. Besides, some authors proposed that during the pining of dislocations on hardening precipitates, some interactions in terms of migration or attraction/repulsion may occur between precipitates and interstitials species dragged by dislocations thus impacting plastic flow and interstitials species distribution respectively [10,11,24]. Knowing the specificities of the DSA regime and of the type C PLC phenomenon in such age-hardenable alloys, an intergranular embrittlement process based on a strain-induced segregation mechanism might be proposed to explain our results. Most likely, in the pure DSA regime (no serrations), dislocations are assumed to drift through grain boundaries interstitial species which might react with oxygen produced and transported by intergranular oxidation process. Such reactions between segregated carbon and oxygen at grain boundaries have already been suggested by Bricknell and Woodford [26,27] during high temperature oxidation of nickel. Conversely, the occurrence of PLC bands is assumed to trap interstitial species in the grains by pinning/pinning off effect on the hardening phases. Consequently, during the OAIC damaging process, two factors are identified to be required: a sufficient cumulated plastic strain for crack initiation and a critical content of dragged reactive species. Therefore, if previous considerations were taken into account, this damaging process established on conventional tensile tests may be invoked to occur nearby the surface of specimen and bring back a possible explanation for the local mechanical loading path dependence of OAIC.

5. Conclusions

Thanks to a dual approach based on a specific experimental specimen and on associated FE calculations, the present study has shown that mechanical loading conditions inducing OAIC initiation randomly observed on conventional tensile tests and defined in terms of strain rate and threshold value of plastic strain may be localized and fulfilled in a delimited area – tip of the V-shaped specimen. Due to the close agreement between FE calculations and mechanical testing in this study, macroscopic key parameters may henceforth be discussed on a polycrystal scale, like the effect of local stress or local strain accumulation.

Moreover, the geometrical and mechanical specificities of the V-shaped specimen, in relation to FE results, make that design a useful and relevant tool in understanding the influence of the localization of gradients of strain and strain rate in the OAIC process. The adaptation of the specific geometrical parameters of the V-shaped specimen, associated with FE calculations, makes possible to cover a larger range of strain rate and to access smoother strain gradients and strain rate and then to make the understanding of the factors impacting OAIC susceptibility concrete. Finally, all this work done on conventional tensile tests and on V-shaped specimens, associated with calculation tools, may be used to further develop structure lifespan assessment.

Acknowledgement

The authors would like to acknowledge the AREVA-NP Company for its financial support.

References

[1] P. Valerio, M. Gao, R.P. Wei, Scripta Metall. Mater. 30 (1994) 1269–1274.
[2] R. Molins, G. Hochstetter, J.C. Chassaigne, E. Andrieu, Acta Mater. 45 (1997) 663–674.
[3] E. Andrieu, A. Pineau, J. Phys. IV 9 (1999) 3–11.
[4] J. Pedron, A. Pineau, Mater. Sci. Eng. 56 (1982) 143–156.
[5] R.P. Wei, C. Miller, Z. Huang, G.W. Simmons, D.G. Harlow, Eng. Fract. Mech. 76 (2009) 715–727.
[6] L. Fournier, D. Delafosse, T. Magnin, Mater. Sci. Eng. A 316 (2001) 166–173.
[7] V. Garat, J.-M. Cloué, D. Poquillon, E. Andrieu, J. Nucl. Mater. 375 (2008) p.95–p.101.
[8] J. Deleume, PhD thesis, INP Toulouse, France, 2007.
[9] B. Ter-Ovanessian, J. Deleume, J.M. Cloué, E. Andrieu, Mater. Sci. Forum 595–598 (2008) 951–958.
[10] W. Chen, M.C. Chaturvedi, Mater. Sci. Eng. A 229 (1997) 163–168.
[11] M.L. Weaver, C.S. Hale, Superalloys 718, 625, 706 and Various Derivatives, TMS, 2001, pp. 421–432.
[12] S. Nalawade, M. Sundararaman, J.B. Singh, R. Kihore, V. Amit, Superalloy 718 and Derivatives, TMS, 2010, pp. 809–823.
[13] J. Kumar, A. Kumar, V. Kumar, Mater. Sci. Eng. A 528 (2011) 4009–4013.
[14] J. Deleume, D. Poquillon, V. Garat, J.M. Cloué, E. Andrieu, Corros. Sci. 50 (2008) 737–743.
[15] D. Wagner, J.C. Moreno, C. Prioul, J.M. Frund, B. Houssin, J. Nucl. Mater. 300 (2002) 178–191.
[16] J. Belotteau, C. Berdin, S. Forest, A. Parrot, C. Prioul, Mater. Sci. Eng. A 526 (2009) 156–165.
[17] L.P. Kubin, Y. Estrin, J. Phys. III 1 (1991) 929–943.
[18] S.L. Mannan, Bull. Mater. Sci. 16 (1993) 561–582.
[19] P. Rodriguez, Bull. Mater. Sci. 6 (1984) 653–663.
[20] A.H. Cottrell, B.A. Bilby, Proc. Phys. Soc. A 62 (1949) 49–62.
[21] A. Van Den Beukel, Acta Metall. 28 (1980) 965–969.
[22] R. Mulford, U. Kocks, Acta Metall. 27 (1979) 1125–1134.
[23] D.M. Riley, P.G. McCormick, Acta Metall. 25 (1977) 181–185.
[24] R. Hayes, W. Hayes, Acta Metall. 30 (1982) 1295–1301.
[25] D. Thevenet, M. Mliha-Touati, A. Zeghloul, Mater. Sci. Eng. A 266 (1999) 175–182.
[26] R. Bricknell, D. Woodford, Acta Metall. 30 (1982) 257–264.
[27] R. Bricknell, D. Woodford, Scripta Mater. 23 (1989) 599–601.